ACS APPLIED POLYMER MATERIALS

pubs.acs.org/acsapm Article

Organic Solar Cells with Large Insensitivity to Donor Polymer Molar Mass across All Acceptor Classes

Stephanie Samson, Jeromy Rech, Lorena Perdigón-Toro, Zhengxing Peng, Safa Shoaee, Harald Ade, Dieter Neher, Martin Stolterfoht, and Wei You*

Cite This: ACS Appl. Polym. Mater. 2020, 2, 5300−5308 Read Online

ACCESS | Metrics & More | Article Recommendations | Supporting Information

ABSTRACT: Donor polymer number-average molar mass (M_n) has long been known to influence organic photovoltaic (OPV) performance via changes in both the polymer properties and the resulting bulk heterojunction morphology. The exact nature of these M_n effects varies from system to system, although there is generally some intermediate M_n that results in optimal performance. Interestingly, our earlier work with the difluorobenzotriazole (FTAZ)-based donor polymer, paired with either N2200 (polymer acceptor) or $PC_{61}BM$ (fullerene acceptor), demonstrated <10% variation in power conversion efficiency and a consistent morphology over a large span of M_n (30 kg/mol to over 100 kg/mol). Would such insensitivity to polymer M_n still hold true when prevailing small molecular acceptors were used with FTAZ? To answer this question, we explored the impact of FTAZ M_n on OPVs with ITIC, a high-performance small-molecule fused-ring electron acceptor (FREA). By probing the photovoltaic characteristics of the resulting OPVs, we show that a similar FTAZ M_n insensitivity is also found in the FTAZ:ITIC system. This study highlights a single-donor polymer which, when paired with an archetypal fullerene, polymer, and FREA, results in systems that are largely insensitive to donor M_n. Our results may have implications in polymer batch-to-batch reproducibility, in particular, relaxing the need for tight M_n control during synthesis.

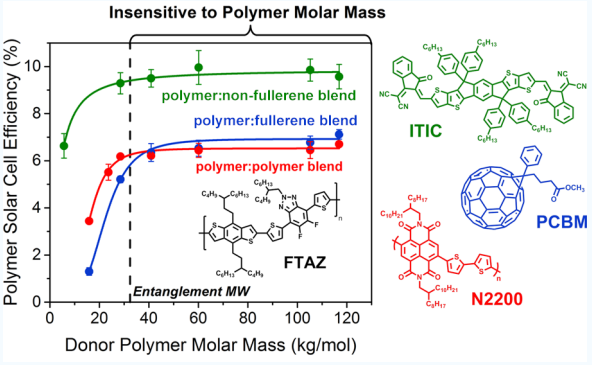

KEYWORDS: *polymer solar cells, conjugated polymers, fullerenes, fluorination, molecular weight, non-fullerene acceptors, power conversion efficiency*

INTRODUCTION

The molecular weight of polymers is perhaps the most important property of a given polymer, which separates polymers from small molecules. Typically, a high molecular weight is required to impart polymers with desirable physical properties, such as thermal stability and mechanical strength.[1,2] Conjugated polymers for bulk heterojunction (BHJ) solar cells are no exception. It has long been recognized that the molecular weight (e.g., number-average molar mass, M_n) of conjugated polymers in BHJ blends has a strong influence on the device performance of such solar cells.[3−6] The M_n of donor polymers affects both the donor properties (e.g., mobility,[7] absorbance,[8] and glass-transition temperature[9]) and BHJ morphology[10] (e.g., domain size and composition,[7,11−13] structure,[14] and surface texture[15,16]). Moreover, the nature and severity of the effects of M_n of a given donor polymer on the performance of BHJ devices can vary from one system to the other when the nature of the paring acceptor (as required by the BHJ) is changed from fullerene derivatives to non-fullerene-based acceptors [including fused-ring electron acceptors (FREAs), other small molecular acceptors, and polymer acceptors].[17,18]

These studies, regardless of the acceptor type, often found that there is some intermediate M_n range for the donor polymer which affords optimal photovoltaic properties, with performance falling off as a consequence of the suboptimal morphology.[5,7,12,19−22] In addition, this optimal M_n range is dependent not only on the chemical nature of the donor polymer but also on the acceptor that is paired with the specific donor in a BHJ blend. For example, consider BHJ organic photovoltaics (OPVs) utilizing the prototypical donor polymer, poly(3-hexylthiophene) (i.e., P3HT). When $PC_{61}BM$ (a fullerene derivative) was used, the maximum power conversion efficiency (PCE) of such BHJ devices was found at an M_n of ∼30 kg/mol for P3HT.[5,19−21] In cases where a FREA acceptor was used, the trend between the M_n of P3HT and PCE can be similar, as with O-IDTBR, or very different, as

Received: September 20, 2020
Accepted: September 23, 2020
Published: October 7, 2020

https://dx.doi.org/10.1021/acsapm.0c01041
ACS Appl. Polym. Mater. 2020, 2, 5300−5308

Scheme 1. Polymerization Reaction (Stille Polycondensation) between the BnDT Moiety and FTAZ Moiety To Form the Donor FTAZ Polymer[a]

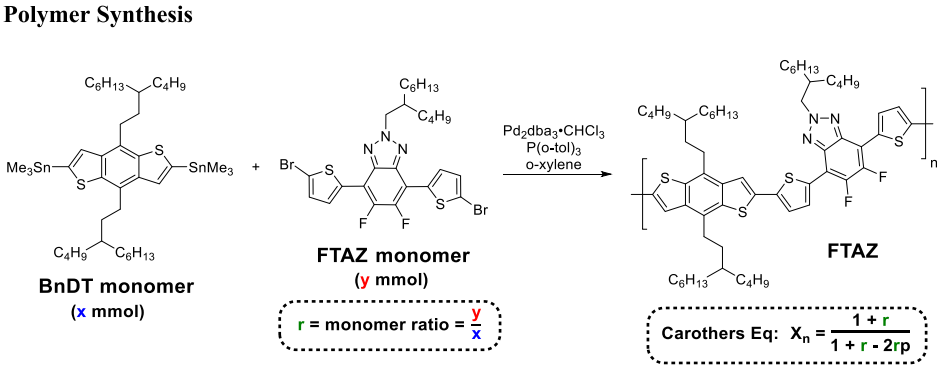

[a]The molar mass is controlled via the Carothers equation, which depends on the ratios of the two monomers (r) and the extent of reaction (p), with the latter assumed to be near unity (p = 0.993) in our case.

with EH-IDTBR.[17] Furthermore, despite P3HT's ubiquity, there is no reported study on the effects of the M_n of P3HT on the BHJ system where P3HT was paired with a polymer acceptor, although such a system had been reported as early as 2007.[23] In fact, to our knowledge, no studies have been done comparing the effects of M_n of the same donor polymer on BHJ solar cells across the three different types of acceptors from fullerene derivatives, to FREAs, to polymer acceptors. Such studies would disclose the differences and similarities of the impact of donor M_n across the three acceptor classes and provide further insights on the fundamental reason why such differences and similarities would occur.

We chose poly(benzodithiophene-alt-dithienyl difluorobenzotriazole) (PBnDT-FTAZ) (i.e., FTAZ going forward) as the donor polymer for this study because we have done extensive works with this particular polymer since its inception in 2011.[24] With collaborators, we had investigated the influence of M_n (FTAZ) on the performance of BHJ OPVs when $PC_{61}BM$ was used as the acceptor, and more recently, with N2200 as the polymer acceptor.[8,11] Thus, to complement the previous work, we set our goal to investigate the impact of M_n (FTAZ) with the remaining acceptor-type FREAs. With this study, we aim to complete our overarching goal of studying the impact of the M_n of a single donor across all three acceptor classes. Specifically, we chose the archetypal FREA, ITIC, in this study. We have measured the photovoltaic and morphological properties of FTAZ:ITIC-based BHJ OPVs utilizing FTAZ of M_n values of 10, 30, 40, 60, 100, and 120 kg/mol (hereafter referred to as 10k, 30k, 40k, 60k, 100k, and 120k FTAZ). We found that an increase in PCE between 10 and 30 kg/mol (M_n of FTAZ) was accompanied by a shift in morphology of the FTAZ:ITIC blends. However, beyond 30 kg/mol, the PCE and morphology of the FTAZ−ITIC blends were rather insensitive to further increases in the M_n of the FTAZ donor polymer, similar to what has been observed with the FTAZ:N2200 and FTAZ:$PC_{61}BM$ systems.

RESULTS AND DISCUSSION

Polymer Synthesis. The polymerization of FTAZ (Scheme 1), along with other donor−acceptor copolymers, is a common step-growth polymerization which can be described by the Carothers equation. In order for the Carothers equation to effectively describe the polymerization, and thus predict the molar mass, both the monomers and palladium catalyst must have very high purity and are recrystallized multiple times prior to use, as described in detail in our earlier work.[11] As there are two monomers, the Carothers equation can control the molar mass by changing the monomer ratio (r; $0 < r \leq 1$); the extent of the reaction (p) is assumed to be near completion (p = 0.993) based on our previous experiences. Pleasingly, the measured M_n from high-temperature gel permeation chromatography (HT-GPC) is close to the theoretical molar mass (Table 1). This observation does not verify only the validity and success of using the Carothers equation in our case; more importantly, the obtained series of FTAZ polymers with different yet controlled M_n offer an excellent system for our study. Further polymerization details can be found in the Supporting Information. All FTAZ polymers in this molar mass range are soluble in common processing solvents of chloroform, chlorobenzene, and toluene (with the assistance of heat).

Table 1. Measured FTAZ Number-Average Molar Mass and Dispersity

FTAZ	M_n (kg/mol)	$Đ$
10k	7.5	2.02
30k	28.5	1.82
40k	40.9	1.96
60k	60.1	1.89
100k	105.2	1.94
120k	116.9	1.91

Device Performance. In order to determine the effect of donor M_n on the efficiency of our model polymer:FREA system, FTAZ:ITIC (1:1 w/w) BHJ devices were fabricated with the inverted architecture of indium tin oxide/ZnO/FTAZ:ITIC/MoO_3/Al and an active layer thickness of ∼90 nm. The resulting photovoltaic characteristics under 1 sun conditions are visualized and tabulated in Figure 1 and Table 2, respectively. Overall, the PCE, short-circuit current density (J_{SC}), open-circuit voltage (V_{OC}), and fill factor (FF) of devices are insensitive to changes in the M_n of FTAZ between ∼30 and 100 kg/mol (Scheme 1, Table 2). However, at a very low M_n, the PCE, J_{SC}, and (to some extent) FF increase between 10 and 30 kg/mol; in contrast, V_{OC} decreases in this range. At a very high M_n (e.g., 120 kg/mol), slight decreases in PCE, V_{OC}, and FF are observed. To understand the origin of the performance difference, we further investigated the device results of these blends.

https://dx.doi.org/10.1021/acsapm.0c01041
ACS Appl. Polym. Mater. 2020, 2, 5300−5308

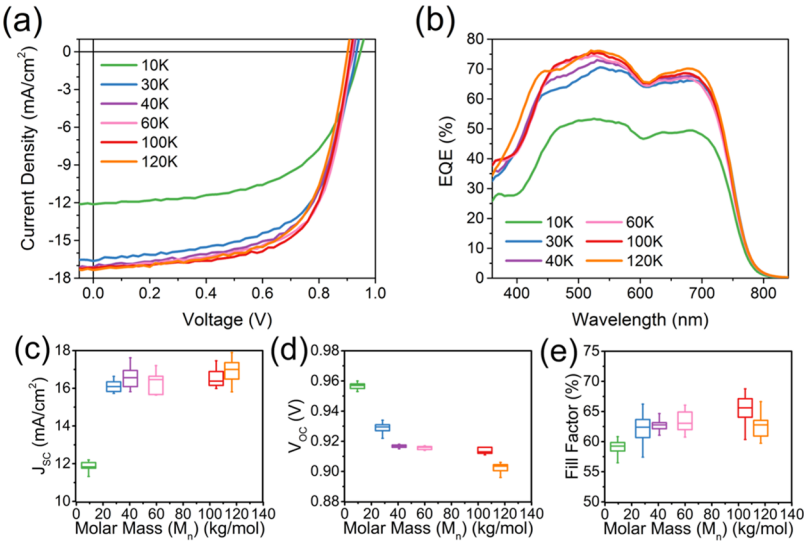

Figure 1. (a) J–V characteristics and (b) EQE of the blends of varying FTAZ M_n with ITIC. Box-and-whisker plots of OPV figures of merit, (c) J_{SC}, (d) V_{OC}, and (e) FF.

Table 2. Photovoltaic Characteristics of FTAZ:ITIC Solar Cells

FTAZ	J_{SC} (mA/cm^2)	V_{OC} (V)	FF (%)	PCE (%)	PCE$_{best}$ (%)	$J_{SC,calc}$ (mA/cm^2)
10k	11.88 ± 0.42	0.956 ± 0.003	58.3 ± 3.4	6.63 ± 0.52	**7.4**	11.23
30k	16.10 ± 0.28	0.929 ± 0.003	62.1 ± 2.5	9.29 ± 0.45	**9.9**	15.09
40k	16.53 ± 0.51	0.916 ± 0.002	62.7 ± 1.0	9.50 ± 0.37	**10.3**	15.49
60k	16.30 ± 0.58	0.916 ± 0.001	63.3 ± 1.8	9.46 ± 0.55	**10.2**	15.48
100k	16.57 ± 0.49	0.914 ± 0.002	65.4 ± 2.1	9.90 ± 0.48	**11.0**	15.79
120k	16.90 ± 0.57	0.903 ± 0.003	62.7 ± 1.9	9.56 ± 0.51	**10.5**	16.12

To begin with, J_{SC} (Figure 1c) increases more than 30% between 10k and 30k FTAZ and then plateaus, with representative J–V characteristic curves (Figure 1a) largely overlapping beyond this point. In fact, the rather dramatic increase of J_{SC} from 10k to 30k is the primary cause for the noticeably increased PCE from 10k to 30k. It is worth noting that this trend is also observed in the FTAZ:PC$_{61}$BM[11] and FTAZ:N2200[8] systems. Absorption trends of the blend films can be found in Figure S1, where all systems show similar and high attenuation coefficients. Previous measurements of neat FTAZ films reveal slight increases in attenuation coefficient with increasing M_n; however, these differences are not enough to account for the drastic change in J_{SC} beyond 30 kg/mol.[8] Furthermore, external quantum efficiency (EQE) (Figure 1b) measurements show similar response profiles for all M_n; however, the maximum response for the 10k polymer-based BHJ device is only ∼50% as opposed to ∼70% for higher M_n polymers, which is consistent with the observed J_{SC} trend with the M_n.

Next, the FF (Figure 1e) also increases over the probed M_n range. Again, an increase is seen between 10k and 30k. Minor increases in FF are seen thereafter, with a slight decrease at very high M_n. We note that this increase in FF between 10k and 30k, also seen in previous studies on FTAZ,[8,11] cannot be strongly attributed to differences in mobility with M_n because resistance-dependent photovoltage (RPV)[25] (Figure S2) shows that mobility is only modestly affected by M_n (1.9×10^{-4} cm^2/V·s for 10k vs 2.8×10^{-4} cm^2/V·s for 100k). This is consistent with previous studies.[8,11] Furthermore, the entanglement M_n as determined through elastic modulus measurements lies slightly below 30 kg/mol.[8] Although entanglement can hinder polymer crystallization,[20] it also increases the incidence of tie chains between crystalline domains.[3] These connections ensure charge transport between crystalline domains,[26] in line with our observed trends in mobility in this study and in previous studies.[11] However, the increase in mobility between low- and high-M_n FTAZ alone is not enough to explain such a marked increase in J_{SC} and FF after 10k.

Unlike J_{SC} and FF, V_{OC} (Figure 1d) appears to decrease with increasing M_n, with the most dramatic changes seen at low M_n. At intermediate M_n, V_{OC} plateaus, followed by a slight drop at very high M_n. V_{OC} is primarily dependent on the energy offset between the donor's highest-occupied molecular orbital (HOMO$_D$) and the acceptor's lowest unoccupied molecular orbital (LUMO$_A$), but it is also affected by recombination dynamics.[27,28] The band gap of FTAZ is not affected by M_n, as previously demonstrated by Li et al.[11] and confirmed here with cyclic voltammetry (CV) measurements (Figure S3a). Moreover, the band gap of the BHJ blend obtained by EQE$_{PV}$ differentiation (dEQE/dE) does not apparently depend on the M_n of FTAZ (Figure S3b). Ultimately, PCE noticeably increases between 10 and 30 kg/mol, plateaus between 30 and 100 kg/mol, and then decreases slightly at 120 kg/mol, with a champion performance of 11%. Although the trend of PCE with M_n largely tracks the trend of J_{SC} with M_n, further investigation of the BHJ morphology and device physics is necessary in order to understand the origin of the J_{SC}, V_{OC}, FF, and PCE trends.

Morphology. As the OPV characteristics are heavily dependent on morphology,[29] we explored the bulk molecular packing and texture of the active layer using synchrotron radiation-based grazing-incidence wide-angle X-ray scattering

https://dx.doi.org/10.1021/acsapm.0c01041
ACS Appl. Polym. Mater. 2020, 2, 5300−5308

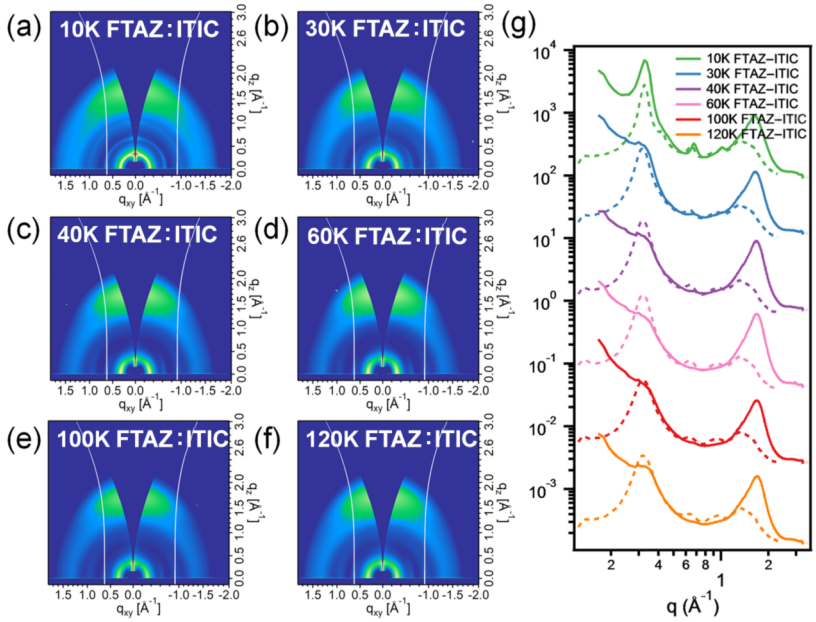

Figure 2. (a–f) 2D GIWAXS patterns and (g) line cuts out-of-plane (solid) and in-plane (dashed) for FTAZ:ITIC blend films with donor M_n of (a) 10, (b) 30, (c) 40, (d) 60, (e) 100, and (f) 120 kg/mol.

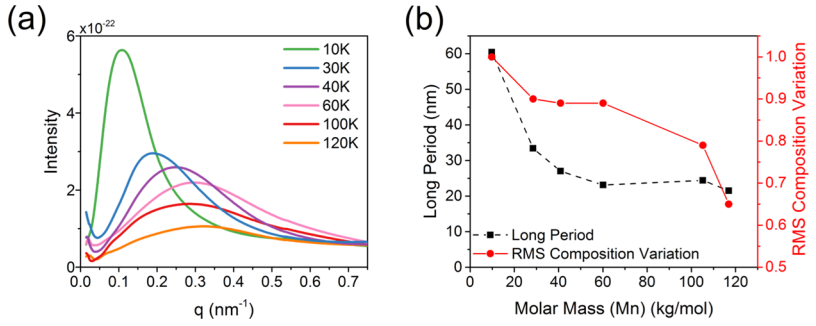

Figure 3. (a) Thickness-normalized RSoXS profiles extracted at 283.4 eV and (b) long period (domain spacing) and root mean square variation (RMS) composition variation (domain purity) for FTAZ:ITIC blends with varying donor M_n.

(GIWAXS) and resonant soft X-ray scattering (RSoXS). GIWAXS was used to extract molecular-scale morphological information both in and out of the sample plane,[30,31] and the collected scattering provides information such as $\pi-\pi$ stacking distance, lamellar spacing, film texture, and crystallinity.[31] Two-dimensional (2D) GIWAXS patterns of neat FTAZ films (Figure S4) revealed relatively low crystallinity with a lamellar stacking peak at q = 0.3 Å^{-1} in-plane (corresponding to a spacing distance of 20.9 Å) and $\pi-\pi$ stacking peaks at $q \sim 1.7$ Å^{-1} out-of-plane (corresponding to a spacing distance of 3.7 Å). Although the morphology was largely similar between the higher M_n FTAZ films, the neat 10k FTAZ film is markedly less ordered, indicative of less preferential packing. Moreover, the in-plane stacking peaks are stronger for higher M_n, suggesting an enhanced preference for the face-on orientation. This is similar to what has been previously observed in our past studies with FTAZ.[8,11] 2D GIWAXS patterns of blend films (Figure 2) demonstrated similar peaks and spacings to the neat films, with a preferential face-on orientation for FTAZ having an M_n over 10 kg/mol. Notably, the 10k FTAZ blend showed little to no preference in the lamellar stacking orientation.

As GIWAXS primarily probes molecular-scale contrast variations (particularly molecular packing), RSoXS was used to probe mesoscale morphological information in the sample plane regarding overall domain characteristics.[32] Here, we extract the long period, or the center-to-center domain spacing, and the relative composition variations of the active layer (formerly called domain purity). By RSoXS, each different M_n of the FTAZ:ITIC blend demonstrated a single size distribution (Figure 3a). In addition, long period and relative composition variations (Figure 3b) decreased with increasing M_n. The 10k polymer blend had the largest domain spacing at ~60 nm, while larger-M_n polymers had domain spacings around ~20 nm. As the exciton diffusion length is ~10 nm,[33] the large spacing in the 10k FTAZ batch hinders charge separation. Furthermore, the relative composition variations show that the 10k blend has the purest domains. Because the 10k blend has both the largest and purest domains, this can result in reduced exciton splitting and will result in a large J_{SC} loss. In addition, domain purity is typically reflected in FF,[34] where excessively impure domains can lead to increased bimolecular recombination[35−38] and excessively pure domains can lead to isolated charge traps.[37] On the other hand, more mixed domains provide an increased interfacial area and percolation pathways beneficial for charge separation and transport, affecting both J_{SC} and FF. The J_{SC} and FF of the 10k

https://dx.doi.org/10.1021/acsapm.0c01041
ACS Appl. Polym. Mater. 2020, 2, 5300−5308

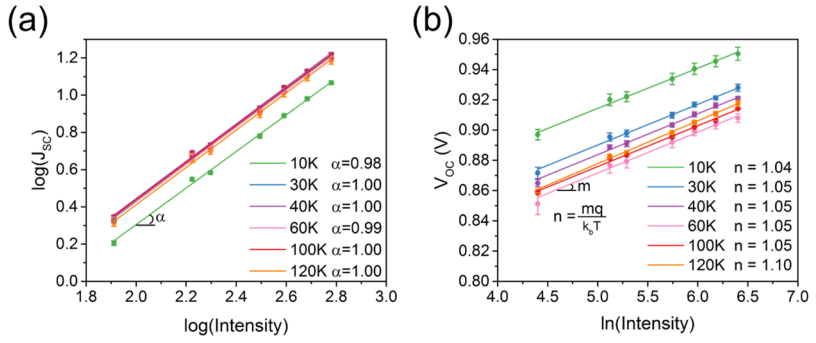

Figure 4. Light intensity measurements for investigating recombination in FTAZ:ITIC blend films. (a) Log−log fitting of J_{SC} vs light intensity (W/m^2) to probe for deviations from weak bimolecular recombination. (b) Semilog fitting of V_{OC} vs light intensity (W/m^2) to determine the recombination order.

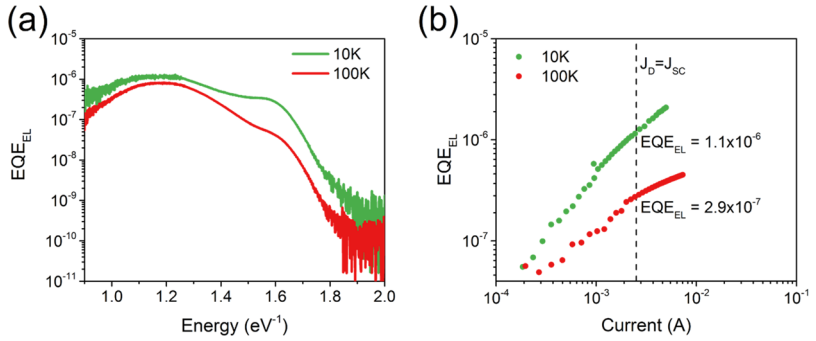

Figure 5. EL spectra of the 10k and 100k FTAZ polymer blends (a) against photon energy and (b) against injection current. The EQE_{EL} for energy loss calculations is taken at an injected current equivalent to the J_{SC} relevant to open-circuit conditions. The graph shows that the EQE_{EL} is approximately ∼3.8 smaller in the 100k FTAZ organic solar cell blend.

polymer are significantly lower than those of higher-M_n polymers despite the high relative domain purity of 10k FTAZ blends. This suggests that the 10k blend's domains may be excessively pure, potentially limiting exciton separation into free carriers. The ultimate effect of the 10k blend's overly large and pure domains is a reduced exciton dissociation efficiency, lowering J_{SC}. On the other hand, the domain purity and spacing were remarkably similar for the intermediate-M_n polymers, although the domain purity decreased slightly for the largest-M_n polymers. This may have contributed to the slight decrease in FF seen at very high M_n. The relatively strong phase segregation in very low-M_n FTAZ blends was also observed in the FTAZ:C_{61}BM system but not in the FTAZ:2200 system. We speculate that low M_n, particularly when the M_n is below the entanglement M_n, could facilitate aggregation of the small molecular acceptors. In contrast, the use of a polymer acceptor may hinder the aggregation of the donor because of the chain entanglements of the acceptor. Despite differences at very low donor M_n, the morphology for all three systems was reasonably invariant for a large range of moderate FTAZ M_n.

In summary, morphological studies reveal that the excessively large and pure domains present in 10k FTAZ blend devices contributed to the markedly low J_{SC} at low M_n. As M_n is increased to intermediate values between 30 and 100 kg/mol, 2D GIWAXS patterns, long period and relative composition variations become relatively constant. While morphological studies have provided insight into our observed J_{SC} and FF trends, the V_{OC} remains unexplained. A hint from the morphology measurements lies in the relative composition variations as the domain purity affects recombination and thus V_{OC}. To clarify the V_{OC} trend, we turn to device physics measurements.

Device Physics. Although analysis of GIWAXS and RSoXS data elucidated trends in J_{SC} and FF, the origin of the observed decrease of V_{OC} from low to very high M_n remains unclear. In order to further investigate this V_{OC} loss, we probed recombination mechanisms of the devices because the recombination losses typically account for the main loss of V_{OC}.[39]

Recombination can be probed by measuring the dependence of $J-V$ characteristics on light intensity. The J_{SC} may have a power law scaling with light intensity (I), $J_{SC} \propto I^{\alpha}$. For relatively low light intensities,[40,41] such as the 1 sun condition, α is typically between 0.9 and 1.[42] Ideally, $\alpha = 1$, signifying that carriers are swept out before recombination at short circuit,[43] although this does not allow to exclude first-order recombination losses.[44] Nevertheless, $\alpha \sim 1$ implies that recombination losses scaling with the second order of the light intensity are absent.[40,41]

On the other hand, V_{oc} can be described by the following equation

$$V_{OC} = \frac{nkT}{q}\ln\left(\frac{J_{SC}}{J_0} + 1\right) \quad (1)$$

where kT is the thermal energy, q is the electric charge, and J_0 is the dark saturation current density. Here, the ideality factor n accounts for the deviation from the ideal bimolecular recombination. Experimentally,[43] the slope of V_{OC} versus $\ln(I)$ can be used to determine n, where I is the light intensity. A slope of unity (i.e., $n = 1$) typically indicates that the

https://dx.doi.org/10.1021/acsapm.0c01041
ACS Appl. Polym. Mater. 2020, 2, 5300−5308

Table 3. Parameters Used for the Calculation of Energy Losses Based on Measured EQE_{EL}

						V_{OC} (V)	
FTAZ	J_{SC} (A/m^2)	$J_{0,rad}$ (A/m^2)	EQE_{EL}	$V_{OC,rad}$ (V)	$\Delta V_{OC,nr}$ (V)	measured	calculated
10k	140	3.3×10^{-20}	1.1×10^{-6}	1.29	0.36	0.92	0.93
100k	170	1.5×10^{-19}	2.9×10^{-7}	1.26	0.39	0.90	0.87

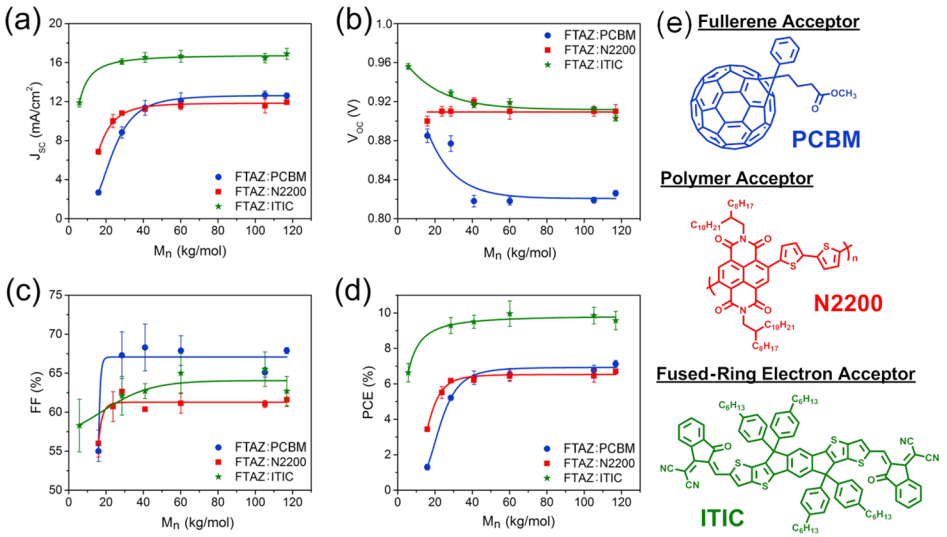

Figure 6. Trends in photovoltaic figures of merit with increasing M_n for the FTAZ:$PC_{61}BM$, FTAZ:N2200, and FTAZ:ITIC systems: (a) J_{SC}, (b) V_{OC}, (c) FF, and (d) PCE. The chemical structure for each electron acceptor is shown in (e). The exact same polymer batches of FTAZ were used for all three systems from 30k to 120k. The solid lines are guides to the eyes.

bimolecular recombination is dominant. Deviations from $n = 1$ indicate the presence of competing recombination processes of different orders. For example, $n \leq 1$ suggests the presence of surface recombination and that the V_{OC} saturates to the built-in voltage, $1 \leq n \leq 2$ implies a combination of bimolecular and trap-assisted recombinations, and $n = 2$ indicates that trap-assisted recombination is dominant.[45,46]

In our system, from the log–log plot of J_{SC} versus I (Figure 4a) and the semilog plot of V_{OC} versus I (Figure 4b), α and n were found to be ~1 for all values of M_n, except for a slight increase in n for 120k FTAZ. This increase in n may have contributed to the slight decrease in FF observed for very high M_n and is also in line with the observed decrease in domain purity. Overall, the light intensity dependence of J_{SC} and V_{OC} indicates that bimolecular recombination is the dominant mechanism for all M_n blends, but it is relatively weak under short-circuit conditions.

To further classify these V_{OC} losses (ΔV_{OC}) from recombination, we can divide ΔV_{OC} into unavoidable radiative ($\Delta V_{OC,rad}$) and avoidable nonradiative ($\Delta V_{OC,nr}$) losses. For this study, the ΔV_{OC} values of 10k and 100k FTAZ (i.e., the M_n values resulting in the lowest and highest PCEs, respectively) were explored. $\Delta V_{OC,nr}$ can be determined experimentally through EQE_{EL} (Figure 5) using

$$\Delta V_{OC,nr} = -\frac{kT}{q}\ln(EQE_{EL}) \tag{2}$$

EQE_{EL} is taken at an injected current such that $J_{inj}(V_{OC}) = J_{SC}$ as $\Delta V_{OC,nr}$ should be evaluated under conditions similar to open-circuit conditions under illumination.[47] Furthermore, the V_{OC} can be calculated by first determining its value in the limit of only radiative recombination ($V_{OC,rad}$)

$$V_{OC,rad} = \frac{kT}{q}\ln\left(\frac{J_{SC}}{J_{0,rad}} + 1\right) \tag{3}$$

and then subtracting the calculated $\Delta V_{OC,nr}$

$$V_{OC} = V_{OC,rad} - \Delta V_{OC,nr} = \frac{E_{CT}}{q} + \frac{kT}{q}\ln\left(\frac{J_{SC}h^3c^2}{fq2\pi(E_{CT} - \lambda)}\right) + \frac{kT}{q}\ln(EQE) \tag{4}$$

where the first two terms in the rightmost expression comprise $V_{OC,rad}$.[48] $J_{0,rad}$ is the radiative current density in the dark due to the blackbody radiation and can be determined by extending the EQE_{PV} using the electroluminescence (EL) spectra (Figure S5).[49,50] Differences in the nonradiative losses account for the majority of the V_{OC} difference between the 10k and 100k FTAZ blends. Table 3 shows that the 10k FTAZ blend has a lower $J_{0,rad}$ and a higher EQE_{EL} than the 100k FTAZ blend, implying that relatively high V_{OC} of the 10k FTAZ blend can thus be attributed to the reduced nonradiative losses using eq 4. Morphologically, the difference in V_{OC} losses may potentially stem from the large and relatively pure domains of the 10k FTAZ blends, where the decreased D:A interfacial area results in decreased radiative[51] and nonradiative[52] recombination. Voltage losses can also be related to the charge-transfer state energy (E_{CT}) through eq 4.[53] However, E_{CT} is difficult to determine because of overlap of the EQE_{PV} with what we ascribe as the singlet emission from the FREA, ITIC at ~1.6 eV[54] (Figure S5). The appearance of a contribution from the singlet excitons in the EL spectra of both blends points to a significant hybridization between charge-transfer states and the first excited singlet, which has

https://dx.doi.org/10.1021/acsapm.0c01041
ACS Appl. Polym. Mater. 2020, 2, 5300–5308

been shown for a number of organic blends.[55] Hybridization results in increased luminescence of the CT state and thereby a decrease in the nonradiative recombination losses.[55] In the case of the 10k and 100k FTAZ blends, the evidence of a stronger singlet "shoulder" in the EL spectrum (Figure 5) suggests a larger coupling to singlet excitons in the 10k FTAZ device, which according to the work of Eisner et al.[55] explains the higher EQE_{EL} values obtained. As for the $J_{0,rad}$, Figure S5 still suggests that E_{CT} could be at slightly higher energies in the 10k FTAZ blend, which could explain the lower $J_{0,rad}$ value and hence the slightly smaller radiative recombination losses.

CONCLUSIONS

We have discovered that the photovoltaic characteristics of FTAZ:ITIC blends are insensitive to M_n within the probed range beyond 30 kg/mol with variations <10%. This trend is not only unusual over such a large M_n range but also consistent with trends seen in the FTAZ:$PC_{61}BM$ and FTAZ:N2200 systems. Thus, this study utilizing the FREA ITIC as the acceptor completes our overarching study on the impact of donor FTAZ M_n with three representative acceptors (Figure 6). Our results from the FTAZ:ITIC system show that increases in FF and J_{SC} from 10k to 30k are primarily attributed to the improved morphology. This morphology is consistent for blend films utilizing 30k or greater FTAZ. A modest increase in mobility is observed despite reduced phase purity, while a smaller long period and a more oriented morphology allows for more efficient exciton dissociation and charge transport. Low-M_n blends demonstrate a higher V_{OC}, which plateaus at intermediate M_n and then continues to decrease. Given the identical band gaps of the neat FTAZ polymers, the increasing energy loss from 10k to 100k is ascribed to lower radiative and nonradiative energy losses in the case of the lower M_n. In summary, together with our earlier works,[8,11] this study demonstrates a single-donor polymer which, when blended with prototypical fullerene ($PC_{61}BM$), polymer (N2200), or FREA (ITIC) acceptors, demonstrates reduced sensitivity of photovoltaic and morphological characteristics over a remarkably wide range of M_n. Although the effects of donor FTAZ M_n observed in this study may not be universal across all possible acceptors, these results suggest that it is possible to achieve efficient and reproducible OPVs with varying acceptor types without the need for stringent M_n control during synthesis, as long as the donor polymer has a sufficiently high M_n. However, the origin of this broad M_n insensitivity is not yet known. The results of the overarching study can serve as a stepping stone for future work to correlate the chemical structure to the observed behavior.

ASSOCIATED CONTENT

Supporting Information

The Supporting Information is available free of charge at https://pubs.acs.org/doi/10.1021/acsapm.0c01041.

Details regarding polymer synthesis and characterization, device fabrication, GIWAXS and RSoXS measurements (including data for neat FTAZ films), RPV measurements, EL spectra, EQE_{EL} measurements, band gap measurements via CV and EQE_{PV} derivatives, and reduced EQE_{PV} and EL spectra (PDF)

AUTHOR INFORMATION

Corresponding Author

Wei You − *Department of Chemistry, University of North Carolina at Chapel Hill, Chapel Hill, North Carolina 27599, United States;* orcid.org/0000-0003-0354-1948; Email: wyou@unc.edu

Authors

Stephanie Samson − *Department of Applied Physical Sciences, University of North Carolina at Chapel Hill, Chapel Hill, North Carolina 27599, United States*

Jeromy Rech − *Department of Chemistry, University of North Carolina at Chapel Hill, Chapel Hill, North Carolina 27599, United States;* orcid.org/0000-0001-7963-9357

Lorena Perdigón-Toro − *Institut für Physik und Astronomie, Universität Potsdam, 14476 Potsdam-Golm, Germany*

Zhengxing Peng − *Department of Physics and ORaCEL, North Carolina State University, Raleigh, North Carolina 27695, United States*

Safa Shoaee − *Institut für Physik und Astronomie, Universität Potsdam, 14476 Potsdam-Golm, Germany*

Harald Ade − *Department of Physics and ORaCEL, North Carolina State University, Raleigh, North Carolina 27695, United States*

Dieter Neher − *Institut für Physik und Astronomie, Universität Potsdam, 14476 Potsdam-Golm, Germany;* orcid.org/0000-0001-6618-8403

Martin Stolterfoht − *Institut für Physik und Astronomie, Universität Potsdam, 14476 Potsdam-Golm, Germany;* orcid.org/0000-0002-4023-2178

Complete contact information is available at: https://pubs.acs.org/10.1021/acsapm.0c01041

Notes

The authors declare no competing financial interest.

ACKNOWLEDGMENTS

S.S., J.R., Z.P., H.A., and W.Y. thank the NSF (CBET-1639429) for financial support. S.S. was supported by a Sofia Kovalevskaya Prize from the Alexander von Humboldt Foundation. The authors would also like to thank Prof. Xiaoli Zhao (Changchun Institute of Applied Chemistry, Chinese Academy of Sciences) for help with HT-GPC measurement. GIWAXS measurements and analysis were supported by the NSF (CBET-1639429). GIWAXS data were obtained at beamline 7.3.3 at the Advanced Light Source (ALS) in the Berkeley National Lab, which is supported by the U.S. Department of Energy (no. DE-AC02-05CH11231).

REFERENCES

(1) Nunes, R. W.; Martin, J. R.; Johnson, J. F. Influence of Molecular Weight and Molecular Weight Distribution on Mechanical Properties of Polymers. *Polym. Eng. Sci.* **1982**, *22*, 205−228.

(2) Seitz, J. T. The Estimation of Mechanical Properties of Polymers from Molecular Structure. *J. Appl. Polym. Sci.* **1993**, *49*, 1331−1351.

(3) Choi, J.; Kim, W.; Kim, D.; Kim, S.; Chae, J.; Choi, S. Q.; Kim, F. S.; Kim, T.-S.; Kim, B. J. Importance of Critical Molecular Weight of Semicrystalline N-Type Polymers for Mechanically Robust, Efficient Electroactive Thin Films. *Chem. Mater.* **2019**, *31*, 3163−3173.

(4) Savagatrup, S.; Printz, A. D.; O'Connor, T. F.; Zaretski, A. V.; Lipomi, D. J. Molecularly Stretchable Electronics. *Chem. Mater.* **2014**, *26*, 3028−3041.

(5) Ma, W.; Kim, J. Y.; Lee, K.; Heeger, A. J. Effect of the Molecular Weight of Poly(3-Hexylthiophene) on the Morphology and Performance of Polymer Bulk Heterojunction Solar Cells. *Macromol. Rapid Commun.* **2007**, *28*, 1776−1780.
(6) Ma, W.; Yang, G.; Jiang, K.; Carpenter, J. H.; Wu, Y.; Meng, X.; McAfee, T.; Zhao, J.; Zhu, C.; Wang, C.; Ade, H.; Yan, H. Influence of Processing Parameters and Molecular Weight on the Morphology and Properties of High-Performance PffBT4T-2OD:PC71BM Organic Solar Cells. *Adv. Energy Mater.* **2015**, *5*, 1501400.
(7) Zhou, N.; Dudnik, A. S.; Li, T. I. N. G.; Manley, E. F.; Aldrich, T. J.; Guo, P.; Liao, H.-C.; Chen, Z.; Chen, L. X.; Chang, R. P. H.; Facchetti, A.; Olvera de la Cruz, M.; Marks, T. J. All-Polymer Solar Cell Performance Optimized via Systematic Molecular Weight Tuning of Both Donor and Acceptor Polymers. *J. Am. Chem. Soc.* **2016**, *138*, 1240−1251.
(8) Balar, N.; Rech, J. J.; Henry, R.; Ye, L.; Ade, H.; You, W.; O'Connor, B. T. The Importance of Entanglements in Optimizing the Mechanical and Electrical Performance of All-Polymer Solar Cells. *Chem. Mater.* **2019**, *31*, 5124−5132.
(9) Savagatrup, S.; Printz, A. D.; Rodriquez, D.; Lipomi, D. J. Best of Both Worlds: Conjugated Polymers Exhibiting Good Photovoltaic Behavior and High Tensile Elasticity. *Macromolecules* **2014**, *47*, 1981−1992.
(10) Grand, C.; Reynolds, J. R. The Interplay between Structure, Processing, and Properties in Organic Photovoltaic Devices: How to Translate Recent Laboratory-Scale Developments to Modules. *MRS Commun.* **2015**, *5*, 155−167.
(11) Li, W.; Yang, L.; Tumbleston, J. R.; Yan, L.; Ade, H.; You, W. Controlling Molecular Weight of a High Efficiency Donor-Acceptor Conjugated Polymer and Understanding Its Significant Impact on Photovoltaic Properties. *Adv. Mater.* **2014**, *26*, 4456−4462.
(12) Khan, J. I.; Ashraf, R. S.; Alamoudi, M. A.; Nabi, M. N.; Mohammed, H. N.; Wadsworth, A.; Firdaus, Y.; Zhang, W.; Anthopoulos, T. D.; McCulloch, I.; Laquai, F. P3HT Molecular Weight Determines the Performance of P3HT:O-IDTBR Solar Cells. *Sol. RRL* **2019**, *3*, 1900023.
(13) Deshmukh, K. D.; Matsidik, R.; Prasad, S. K. K.; Connal, L. A.; Liu, A. C. Y.; Gann, E.; Thomsen, L.; Hodgkiss, J. M.; Sommer, M.; McNeill, C. R. Tuning the Molecular Weight of the Electron Accepting Polymer in All-Polymer Solar Cells: Impact on Morphology and Charge Generation. *Adv. Funct. Mater.* **2018**, *28*, 1707185.
(14) Nicolet, C.; Deribew, D.; Renaud, C.; Fleury, G.; Brochon, C.; Cloutet, E.; Vignau, L.; Wantz, G.; Cramail, H.; Geoghegan, M.; Hadziioannou, G. Optimization of the Bulk Heterojunction Composition for Enhanced Photovoltaic Properties: Correlation between the Molecular Weight of the Semiconducting Polymer and Device Performance. *J. Phys. Chem. B* **2011**, *115*, 12717−12727.
(15) Osaka, I.; Saito, M.; Mori, H.; Koganezawa, T.; Takimiya, K. Drastic Change of Molecular Orientation in a Thiazolothiazole Copolymer by Molecular-Weight Control and Blending with PC 61BM Leads to High Efficiencies in Solar Cells. *Adv. Mater.* **2012**, *24*, 425−430.
(16) Xiong, W.; Qi, F.; Liu, T.; Huo, L.; Xue, X.; Bi, Z.; Zhang, Y.; Ma, W.; Wan, M.; Liu, J.; Sun, Y. Controlling Molecular Weight to Achieve High-Efficient Polymer Solar Cells With Unprecedented Fill Factor of 79% Based on Non-Fullerene Small Molecule Acceptor. *Sol. RRL* **2018**, *2*, 1800129.
(17) Wadsworth, A.; Hamid, Z.; Bidwell, M.; Ashraf, R. S.; Khan, J. I.; Anjum, D. H.; Cendra, C.; Yan, J.; Rezasoltani, E.; Guilbert, A. A. Y. Y.; Azzouzi, M.; Gasparini, N.; Bannock, J. H.; Baran, D.; Wu, H.; de Mello, J. C.; Brabec, C. J.; Salleo, A.; Nelson, J.; Laquai, F.; McCulloch, I. Progress in Poly (3-Hexylthiophene) Organic Solar Cells and the Influence of Its Molecular Weight on Device Performance. *Adv. Energy Mater.* **2018**, *8*, 1801001.
(18) Choi, J.; Kim, W.; Kim, S.; Kim, T.-S.; Kim, B. J. Influence of Acceptor Type and Polymer Molecular Weight on the Mechanical Properties of Polymer Solar Cells. *Chem. Mater.* **2019**, *31*, 9057−9069.
(19) Mauer, R.; Kastler, M.; Laquai, F. The Impact of Polymer Regioregularity on Charge Transport and Efficiency of P3HT:PCBM Photovoltaic Devices. *Adv. Funct. Mater.* **2010**, *20*, 2085−2092.
(20) Ballantyne, A. M.; Chen, L.; Dane, J.; Hammant, T.; Braun, F. M.; Heeney, M.; Duffy, W.; McCulloch, I.; Bradley, D. D. C.; Nelson, J. The Effect of Poly(3-Hexylthiophene) Molecular Weight on Charge Transport and the Performance of Polymer: Fullerene Solar Cells. *Adv. Funct. Mater.* **2008**, *18*, 2373−2380.
(21) Spoltore, D.; Vangerven, T.; Verstappen, P.; Piersimoni, F.; Bertho, S.; Vandewal, K.; Van Den Brande, N.; Defour, M.; Van Mele, B.; De Sio, A.; Parisi, J.; Lutsen, L.; Vanderzande, D.; Maes, W.; Manca, J. V. Effect of Molecular Weight on Morphology and Photovoltaic Properties in P3HT:PCBM Solar Cells. *Org. Electron.* **2015**, *21*, 160−170.
(22) Huang, Z.; Fregoso, E. C.; Dimitrov, S.; Tuladhar, P. S.; Soon, Y. W.; Bronstein, H.; Meager, I.; Zhang, W.; McCulloch, I.; Durrant, J. R. Optimisation of Diketopyrrolopyrrole:Fullerene Solar Cell Performance through Control of Polymer Molecular Weight and Thermal Annealing. *J. Mater. Chem. A* **2014**, *2*, 19282−19289.
(23) McNeill, C. R.; Abrusci, A.; Zaumseil, J.; Wilson, R.; McKiernan, M. J.; Burroughes, J. H.; Halls, J. J. M.; Greenham, N. C.; Friend, R. H. Dual Electron Donor/Electron Acceptor Character of a Conjugated Polymer in Efficient Photovoltaic Diodes. *Appl. Phys. Lett.* **2007**, *90*, 193506.
(24) Price, SC; Stuart, AC; Yang, L.; Zhou, H.; You, W. Fluorine Substituted Conjugated Polymer of Medium Band Gap Yields 7% Efficiency in Polymer-Fullerene Solar Cells. *J. Am. Chem. Soc.* **2011**, *133*, 4625−31.
(25) Philippa, B.; Stolterfoht, M.; Burn, P. L.; Juška, G.; Meredith, P.; White, R. D.; Pivrikas, A. The Impact of Hot Charge Carrier Mobility on Photocurrent Losses in Polymer-Based Solar Cells. *Sci. Rep.* **2014**, *4*, 5695.
(26) Noriega, R.; Rivnay, J.; Vandewal, K.; Koch, F. P. V.; Stingelin, N.; Smith, P.; Toney, M. F.; Salleo, A. A General Relationship between Disorder, Aggregation and Charge Transport in Conjugated Polymers. *Nat. Mater.* **2013**, *12*, 1038−1044.
(27) Gaspar, H.; Figueira, F.; Pereira, L.; Mendes, A.; Viana, J.; Bernardo, G.; Gaspar, H.; Figueira, F.; Pereira, L.; Mendes, A.; Viana, J. C.; Bernardo, G. Recent Developments in the Optimization of the Bulk Heterojunction Morphology of Polymer: Fullerene Solar Cells. *Materials* **2018**, *11*, 2560.
(28) Benduhn, J.; Tvingstedt, K.; Piersimoni, F.; Ullbrich, S.; Fan, Y.; Tropiano, M.; McGarry, K. A.; Zeika, O.; Riede, M. K.; Douglas, C. J.; Barlow, S.; Marder, S. R.; Neher, D.; Spoltore, D.; Vandewal, K. Intrinsic Non-Radiative Voltage Losses in Fullerene-Based Organic Solar Cells. *Nat. Energy* **2017**, *2*, 17053.
(29) Jiao, X.; Ye, L.; Ade, H. Quantitative Morphology−Performance Correlations in Organic Solar Cells: Insights from Soft X-Ray Scattering. *Adv. Energy Mater.* **2017**, *7*, 1700084.
(30) Hexemer, A.; Müller-Buschbaum, P. Advanced Grazing-Incidence Techniques for Modern Soft-Matter Materials Analysis. *IUCrJ* **2015**, *2*, 106−125.
(31) Müller-Buschbaum, P. The Active Layer Morphology of Organic Solar Cells Probed with Grazing Incidence Scattering Techniques. *Adv. Mater.* **2014**, *26*, 7692−7709.
(32) Ye, L.; Stuard, S. J.; Ade, H. X-Ray Scattering Characterization of Polymer Semiconductors. *Conjugated Polymers: Properties, Processing, and Applications*; Reynolds, J. R.; Thompson, B. C.; Skotheim, T. A., Eds.; CRC Press: Florida, 2019; pp 427−458.
(33) Halls, J. J. M.; Pichler, K.; Friend, R. H.; Moratti, S. C.; Holmes, A. B. Exciton Diffusion and Dissociation in a Poly(p-phenylenevinylene)/C 60 Heterojunction Photovoltaic Cell. *Appl. Phys. Lett.* **1996**, *68*, 3120−3122.
(34) Huang, W.; Gann, E.; Chandrasekaran, N.; Thomsen, L.; Prasad, S. K. K.; Hodgkiss, J. M.; Kabra, D.; Cheng, Y.-B.; McNeill, C. R. Isolating and Quantifying the Impact of Domain Purity on the Performance of Bulk Heterojunction Solar Cells. *Energy Environ. Sci.* **2017**, *10*, 1843−1853.

https://dx.doi.org/10.1021/acsapm.0c01041
ACS Appl. Polym. Mater. 2020, 2, 5300−5308

(35) Mukherjee, S.; Jiao, X.; Ade, H. Charge Creation and Recombination in Multi-Length Scale Polymer:Fullerene BHJ Solar Cell Morphologies. *Adv. Energy Mater.* **2016**, *6*, 1600699.
(36) Ye, L.; Zhao, W.; Li, S.; Mukherjee, S.; Carpenter, J. H.; Awartani, O.; Jiao, X.; Hou, J.; Ade, H. High-Efficiency Nonfullerene Organic Solar Cells: Critical Factors That Affect Complex Multi-Length Scale Morphology and Device Performance. *Adv. Energy Mater.* **2017**, *7*, 1602000.
(37) Ma, W.; Ye, L.; Zhang, S.; Hou, J.; Ade, H. Competition between Morphological Attributes in the Thermal Annealing and Additive Processing of Polymer Solar Cells. *J. Mater. Chem. C* **2013**, *1*, 5023−5030.
(38) Ma, W.; Tumbleston, J. R.; Wang, M.; Gann, E.; Huang, F.; Ade, H. Domain Purity, Miscibility, and Molecular Orientation at Donor/Acceptor Interfaces in High Performance Organic Solar Cells: Paths to Further Improvement. *Adv. Energy Mater.* **2013**, *3*, 864−872.
(39) Elumalai, N. K.; Uddin, A. Open Circuit Voltage of Organic Solar Cells: An in-Depth Review. *Energy Environ. Sci.* **2016**, *9*, 391−410.
(40) Koster, L. J. A.; Kemerink, M.; Wienk, M. M.; Maturová, K.; Janssen, R. A. J. Quantifying Bimolecular Recombination Losses in Organic Bulk Heterojunction Solar Cells. *Adv. Mater.* **2011**, *23*, 1670−1674.
(41) Stolterfoht, M.; Armin, A.; Philippa, B.; White, R. D.; Burn, P. L.; Meredith, P.; Juška, G.; Pivrikas, A. Photocarrier Drift Distance in Organic Solar Cells and Photodetectors. *Sci. Rep.* **2015**, *5*, 9949.
(42) Koster, L. J. A.; Mihailetchi, V. D.; Ramaker, R.; Xie, H.; Blom, P. W. Light Intensity Dependence of Open-Circuit Voltage and Short-Circuit Current of Polymer/Fullerene Solar Cells. *Org. Optoelectron.* **2006**, *6192*, 61922G.
(43) Kyaw, A. K. K.; Wang, D. H.; Gupta, V.; Leong, W. L.; Ke, L.; Bazan, G. C.; Heeger, A. J. Intensity Dependence of Current-Voltage Characteristics and Recombination in High-Efficiency Solution-Processed Small-Molecule Solar Cells. *ACS Nano* **2013**, *7*, 4569−4577.
(44) Würfel, U.; Perdigón-Toro, L.; Kurpiers, J.; Wolff, C. M.; Caprioglio, P.; Rech, J. J.; Zhu, J.; Zhan, X.; You, W.; Shoaee, S.; Neher, D.; Stolterfoht, M. Recombination between Photogenerated and Electrode-Induced Charges Dominates the Fill Factor Losses in Optimized Organic Solar Cells. *J. Phys. Chem. Lett.* **2019**, *10*, 3473−3480.
(45) Cowan, S. R.; Roy, A.; Heeger, A. J. Recombination in Polymer-Fullerene Bulk Heterojunction Solar Cells. *Phys. Rev. B: Condens. Matter Mater. Phys.* **2010**, *82*, 245207.
(46) Tress, W.; Yavari, M.; Domanski, K.; Yadav, P.; Niesen, B.; Correa Baena, J. P.; Hagfeldt, A.; Graetzel, M. Interpretation and Evolution of Open-Circuit Voltage, Recombination, Ideality Factor and Subgap Defect States during Reversible Light-Soaking and Irreversible Degradation of Perovskite Solar Cells. *Energy Environ. Sci.* **2018**, *11*, 151−165.
(47) Vandewal, K.; Benduhn, J.; Nikolis, V. C. How to Determine Optical Gaps and Voltage Losses in Organic Photovoltaic Materials. *Sustainable Energy Fuels* **2018**, *2*, 538−544.
(48) Vandewal, K.; Tvingstedt, K.; Gadisa, A.; Inganäs, O.; Manca, J. V. Relating the Open-Circuit Voltage to Interface Molecular Properties of Donor:Acceptor Bulk Heterojunction Solar Cells. *Phys. Rev. B: Condens. Matter Mater. Phys.* **2010**, *81*, 125204.
(49) Liu, Z.; Krückemeier, L.; Krogmeier, B.; Klingebiel, B.; Márquez, J. A.; Levcenko, S.; Öz, S.; Mathur, S.; Rau, U.; Unold, T.; Kirchartz, T. Open-Circuit Voltages Exceeding 1.26 v in Planar Methylammonium Lead Iodide Perovskite Solar Cells. *ACS Energy Lett.* **2019**, *4*, 110−117.
(50) Yao, J.; Kirchartz, T.; Vezie, M. S.; Faist, M. A.; Gong, W.; He, Z.; Wu, H.; Troughton, J.; Watson, T.; Bryant, D.; Nelson, J. Quantifying Losses in Open-Circuit Voltage in Solution-Processable Solar Cells. *Phys. Rev. Appl.* **2015**, *4*, 014020.
(51) Lipomi, D. J.; Chong, H.; Vosgueritchian, M.; Mei, J.; Bao, Z. Toward Mechanically Robust and Intrinsically Stretchable Organic Solar Cells: Evolution of Photovoltaic Properties with Tensile Strain. *Sol. Energy Mater. Sol. Cells* **2012**, *107*, 355−365.
(52) Tang, Z.; Wang, J.; Melianas, A.; Wu, Y.; Kroon, R.; Li, W.; Ma, W.; Andersson, M. R.; Ma, Z.; Cai, W.; Tress, W.; Inganäs, O. Relating Open-Circuit Voltage Losses to the Active Layer Morphology and Contact Selectivity in Organic Solar Cells. *J. Mater. Chem. A* **2018**, *6*, 12574−12581.
(53) Azzouzi, M.; Yan, J.; Kirchartz, T.; Liu, K.; Wang, J.; Wu, H.; Nelson, J. Nonradiative Energy Losses in Bulk-Heterojunction Organic Photovoltaics. *Phys. Rev. X* **2018**, *8*, 031055.
(54) Kotova, M. S.; Londi, G.; Junker, J.; Dietz, S.; Privitera, A.; Tvingstedt, K.; Beljonne, D.; Sperlich, A.; Dyakonov, V. On the Absence of Triplet Exciton Loss Pathways in Non-Fullerene Acceptor Based Organic Solar Cells. *Mater. Horiz.* **2020**, *7*, 1641−1649.
(55) Eisner, F. D.; Azzouzi, M.; Fei, Z.; Hou, X.; Anthopoulos, T. D.; Dennis, T. J. S.; Heeney, M.; Nelson, J. Hybridization of Local Exciton and Charge-Transfer States Reduces Nonradiative Voltage Losses in Organic Solar Cells. *J. Am. Chem. Soc.* **2019**, *141*, 6362−6374.

https://dx.doi.org/10.1021/acsapm.0c01041
ACS Appl. Polym. Mater. 2020, 2, 5300−5308